



Ultrafast dynamic contrast-enhanced breast MRI: association with pathologic complete response in neoadjuvant treatment of breast cancer

Ji Hee Kim¹ · Vivian Youngjean Park² · Hye Jung Shin³ · Min Jung Kim² · Jung Hyun Yoon²

Received: 8 July 2021 / Revised: 2 November 2021 / Accepted: 15 December 2021 / Published online: 22 January 2022
© The Author(s), under exclusive licence to European Society of Radiology 2022

Abstract

Objectives The purpose of this study was to investigate whether pretreatment kinetic features from ultrafast DCE-MRI are associated with pathological complete response (pCR) in patients with invasive breast cancer and according to immunohistochemistry (IHC) subtype.

Methods Between August 2018 and June 2019, 256 consecutive breast cancer patients (mean age, 50.2 years; range, 25–86 years) who underwent both ultrafast and conventional DCE-MRI and surgery following neoadjuvant chemotherapy were included. DCE-MRI kinetic features were obtained from pretreatment MRI data. Time-to-enhancement, maximal slope (MS), and volumes at U1 and U2 (U1, time point at which the lesion starts to enhance; U2, subsequent time point after U1) were derived from ultrafast MRI. Logistic regression analysis was performed to identify factors associated with pCR.

Results Overall, 41.4% of all patients achieved pCR. None of the kinetic features was associated with pCR when including all cancers. Among ultrafast DCE-MRI kinetic features, a lower MS (OR, 0.982; $p=0.040$) was associated with pCR at univariable analysis in hormone receptor (HR)–positive cancers. In triple-negative cancers, a higher volume ratio U1/U2 was associated with pCR at univariable (OR, 11.787; $p=0.006$) and multivariable analysis (OR, 14.811; $p=0.005$). Among conventional DCE-MRI kinetic features, a lower peak enhancement (OR, 0.993; $p=0.031$) and a lower percentage of washout (OR, 0.904; $p=0.039$) was associated with pCR only in HR-positive cancers at univariable analysis.

Conclusions A higher volume ratio of U1/U2 derived from ultrafast DCE-MRI was independently associated with pCR in triple-negative invasive breast cancer.

Key Points

- The ratio of tumor volumes obtained at the first (U1) and second time points (U2) of enhancement was independently associated with pCR in triple-negative invasive breast cancers.
- Ultrafast MRI has the potential to improve accuracy in predicting treatment response and personalizing therapy.

Keywords Neoadjuvant therapy · Magnetic resonance imaging · Breast neoplasms · Kinetics · Immunohistochemistry

Abbreviations

CAD	Computer-aided diagnosis
CI	Confidence interval
ER	Estrogen receptor
FOV	Field of view
HER2	Human epidermal growth factor receptor type 2
HR	Hormone receptor
ICC	Intraclass correlation coefficient
IHC	Immunohistochemistry
MS	Maximal slope
NAC	Neoadjuvant chemotherapy
OR	Odds ratio
pCR	Pathological complete response

✉ Vivian Youngjean Park
VIVIANPARK0116@yuhs.ac

¹ Department of Radiology, College of Medicine, CHA Ilsan Medical Center, CHA University, Pocheon, Korea

² Department of Radiology, College of Medicine, Severance Hospital, Research Institute of Radiological Science, Yonsei University, 50 Yonsei-ro, Seodaemun-gu, Seoul 03722, Korea

³ Department of Biomedical Systems Informatics, Biostatistics Collaboration Unit, College of Medicine, Yonsei University, Seoul, Korea

PR Progesterone receptor
TTE Time-to-enhancement

Introduction

Neoadjuvant chemotherapy (NAC) has become standard treatment in locally advanced breast cancer, and is now used for triple-negative and human epidermal growth factor receptor 2 (HER2)-positive breast cancer even in early-stage cancer. As previous trials have shown that patients with HER2-positive or triple-negative breast cancer and residual disease after NAC derive a survival benefit from switching to specific adjuvant treatments [1], the prognostic role of accurately assessing pathologic complete response (pCR) has also become increasingly important. Dynamic contrast-enhanced (DCE)-MRI has been widely used as an imaging modality for evaluating tumor response in breast cancer after NAC, and has been reported to show superior performance to mammography and ultrasonography in depicting residual disease [2, 3]. However, early prediction of response has been reported to be less accurate than post-treatment prediction [4]. Predicting response earlier, preferably even before the initiation of treatment, expands clinical applications by allowing personalized treatment modification and avoidance of ineffective treatment.

Despite growing interest in expanding the role of MRI in both screening and diagnostic imaging, access to MRI is limited mostly due to cost and scan time issues. Therefore, attempts to shorten MRI to make it more accessible have recently gained momentum, including ultrafast MRI [5]. Breast ultrafast DCE-MRI has a very high temporal resolution, ranging from approximately 4 to 7 s, and provides kinetic information at very early time points [6, 7]. Several previous studies have reported that such early kinetic information demonstrates comparable accuracy in discriminating benign breast lesions from malignant lesions compared to the kinetic curve analysis derived from conventional DCE-MRI, implying that the very early phase from ultrafast DCE-MRI may substitute for the conventional DCE-MRI delayed phase [7, 8]. In addition, a recent study has also reported that ultrafast DCE-MRI kinetic parameters were associated with tumor aggressiveness [8]. However, to the best of our knowledge, no studies have been published regarding the association between early kinetic parameters derived from pretreatment ultrafast DCE-MRI and pCR after NAC in patients with invasive breast cancer. As ultrafast MRI can be combined with conventional DCE-MRI, combining kinetic information from both could improve response prediction. In addition, as sensitivity to NAC differs according to cancer subtype with pCR rates ranging from 0.3 to 50.3% [9, 10], kinetic parameters associated with treatment response may also differ according to tumor subtype.

Thus, the purpose of our study was to investigate whether pretreatment kinetic features from ultrafast DCE-MRI are associated with pCR in patients with invasive breast cancer and according to immunohistochemistry (IHC) subtype.

Materials and methods

Study population

This retrospective study was approved by the Institutional Review Board, and the requirement for informed consent was waived. We retrospectively reviewed breast MRI studies obtained in our institution between August 2018 and June 2019. From the breast MRI database, we identified 1709 consecutive women with breast cancer who underwent preoperative breast MRI. During the study period, all women who underwent preoperative MRI for newly diagnosed breast cancer were imaged with a combined protocol including ultrafast and conventional DCE-MRI. Among them, 266 women had received NAC. Among these patients, we excluded those who did not undergo surgery at our institution ($n=3$) and those with inadequate computer-aided diagnosis (CAD)-generated images for analysis ($n=7$). Inadequate CAD-generated images included presence of motion artifacts ($n=5$) or tumors located at the far peripheral breast ($n=2$) for which automatic segmentation and angiovolume calculation by the CAD system was not possible. Finally, 256 women (mean age, 50.2 years; age range, 25–86 years) with 256 invasive breast cancers who underwent NAC and surgery were included in this study.

MRI protocol

MRI examinations were performed using a 3-T MRI scanner (Ingenia or Ingenia CX, Philips Healthcare) with a dedicated 16-channel bilateral breast coil with the patient in the prone position. The dynamic series were preceded by sequences including a three-plane localizing sequence, axial bilateral modified Dixon turbo spin echo T2-weighted sequences, and an axial diffusion-weighted sequence. The ultrafast and

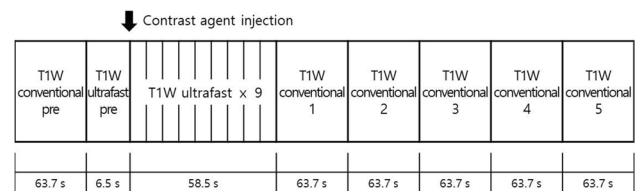


Fig. 1 DCE-MRI protocols for ultrafast and conventional axial MRI. DCE, dynamic contrast-enhanced; DWI, diffusion-weighted imaging; s, seconds; T1W, T1-weighted

conventional DCE-MRI protocol is shown in Fig. 1. For the dynamic series, we first obtained conventional, precontrast images, and then obtained pre- and post-contrast images with the ultrafast protocol before performing post-contrast conventional DCE-MRI. The ultrafast sequence obtained a total of 10 phase images with a 6.5-s temporal resolution, with 9 phases acquired immediately after and during contrast injection. Gadobutrol (Gadovist, Bayer Healthcare) was intravenously injected at a dose of 0.1 mmol/kg of body weight and at a rate of 2 mL/s followed by a 20-mL saline flush. Subsequently, conventional post-contrast image acquisition was performed immediately after completion of the ultrafast sequence, which consisted of five post-contrast axial phases. An enhanced T1-weighted high-resolution isotropic volume examination (eTHRIVE) sequence with a 63.7-s temporal resolution was used for conventional DCE-MRI. Therefore, the first and fifth conventional post-contrast image was obtained at approximately 58.5 s and 313.3 s after contrast injection, respectively. Details regarding acquisition parameters for axial ultrafast and conventional DCE-MRI are presented in Table 1. After the completion of axial post-contrast sequences, we obtained additional images with a T1-weighted delayed post-contrast sequence in the sagittal plane, including the full range of the axilla (TR/TE, 4.1/2.1 ms; FOV, 250×250 mm; matrix, 320×320 mm; thickness, 3 mm).

Conventional MRI analysis

One dedicated breast radiologist (V.Y.P, with 7 years of subspecialty experience in breast imaging) reviewed

conventional DCE-MRI according to the American College of Radiology Breast Imaging-Reporting and Data System [11], and categorized lesions into masses and nonmass enhancement (with or without a mass). Multiplicity was defined as findings highly suspicious for additional sites of malignancy within the ipsilateral breast, based on tissue confirmation or imaging. In women with multifocal or multicentric disease, only the largest biopsy-proven tumors were included for analysis. Tumor size, which was measured as the maximum diameter of the enhancing tumor, was recorded from the radiological report.

All conventional DCE-MRI data were transferred to a commercially available CAD system (CADstream, version 6.0; Merge Healthcare, Inc.). Tumor enhancement kinetics were retrospectively assessed by using the CAD system. When comparing the precontrast and first contrast-enhanced series, a 50% enhancement threshold was selected. The system automatically segmented the tumors in 3D and calculated the angiovolume (total enhancing lesion volume), peak enhancement value (the highest pixel signal intensity in the first contrast-enhanced series), and delayed enhancement profiles (proportions of washout, plateau, and persistent enhancement components). A color-coded map was generated based on changes in pixel values between initial and delayed contrast-enhanced series. The washout type consisted of a decreased pixel signal intensity at the last contrast-enhanced series of more than 10% from the first contrast-enhanced series. The persistent type consisted of an increased pixel signal intensity at the last contrast-enhanced series of more than 10% from the first contrast-enhanced series. The plateau type consisted of a change in either

Table 1 Acquisition parameters for ultrafast and conventional axial DCE-MRI

Parameter	Ultrafast	Conventional
Sequence	T1-TFE	eTHRIVE
TR/TE (msec)	3.5/1.7	4.2/2.1
Field of view (mm ²)	250×320	250×320
Matrix size	320×410	320×410
Slice thickness (mm)	3.0	3.0
Voxel size (mm ³)	0.78×0.78×3.0	0.78×0.78×3.0
Temporal resolution (seconds)	6.5	63.7
SENSE acceleration factor (right-left)	4	2.4
SENSE acceleration factor (foot to head)	1.3	1
Number of slices	50	50
Flip angle (°)	12	17
Sharing method	CENTRA-Keyhole Central size (%): 50 Reference scan: first	
Fat suppression method	SPAIR	SPAIR

SENSE = sensitivity encoding, CENTRA = contrast-enhanced timing robust angiography, SPAIR = spectral attenuated inversion recovery, TFE = turbo field echo, eTHRIVE = enhanced T1-weighted high-resolution isotropic volume examination, TR = repetition time, TE = echo time

direction less than 10% from the first contrast-enhanced series. On the basis of delayed enhancement profiles, we recorded the percentage of washout enhancing components within each tumor.

Ultrafast DCE-MRI analysis

Analyses of ultrafast DCE-MRI parameters were performed on a workstation (Aquarius iNtuition Viewer; TeraRecon). Using 10 phases of ultrafast-DCE MR images, 9 subtracted images were obtained by subtracting the first (precontrast) phase from each of the other 9 phases. Sequential maximum-intensity projection (MIP) images were generated for each time point. Time-to-enhancement (TTE) was defined as “the time point where the lesion starts to enhance minus the time point where the aorta starts to enhance” [8]. Two readers (V.Y.P and J.H.K, with 7 and 6 years of experience, respectively) evaluated TTE in consensus based on the MIP images. When it was difficult to visually decide the time point based on MIP images, we determined it as the point where the washin curve starts to rise with the aid of the software [12]. The maximal slope (MS) was determined as the slope of the tangent (percentage relative enhancement/second [%/s]) along the steepest part of the curve [8], which was automatically calculated by the software. One reader (V.Y.P) placed a circular region of interest (ROI) of 3×3 mm for the strongest and most rapidly enhancing part of the tumor (henceforth, referred to as MS_3mm) and also manually drew a ROI over the enhancing portion of the representative slice of the tumor on the post-contrast ultrafast MRI (henceforth, referred to as MS).

In addition, we measured the volume of each tumor on ultrafast DCE-MRI. U1 was defined as the time point at which the lesion starts to enhance and U2 was defined as the subsequent time point after the lesion starts to enhance. After visually reviewing the cases, we found that the tumor volumes generally did not significantly differ between U2 and later ultrafast DCE-MRI phases. Therefore, we chose to obtain volume data from time points U1 and U2 (Figs. 2 and 3). One breast radiologist (V.Y.P) manually segmented the tumors at U1 and U2 on subtraction images using the software (Aquarius iNtuition Viewer). The enhancing portion of the tumor was manually outlined on each slice containing the tumor, and then the tumor volume was automatically calculated by the software. To evaluate interobserver reproducibility, another breast radiologist (J.H.K) independently performed tumor segmentation on 40 randomly chosen lesions. In addition, we calculated the ratios of tumor volume from each time point: volume ratio U1/U2, the ratio of tumor volume at U1 to tumor volume at U2; volume ratio U1/CAD, the ratio of tumor volume at U1 to angiovolume calculated by the CAD system (CADstream); and U2/CAD, the ratio of tumor volume at U2 to angiovolume calculated by the CAD system.

Clinicopathologic data collection

Clinicopathologic data (patient age, preoperative clinical lymph node status, treatment, and histopathological information) were collected from medical records. Clinically node positive was defined as positive signs of axillary lymph node metastases on either preoperative axillary ultrasound or cyto-/histopathology [13]. The histologic type and IHC subgroup were assessed based on pretreatment core biopsy specimens. The positivity for each of the biomarkers was defined according to the American Society of Clinical Oncology (ASCO)/College of American Pathologists (CAP) guidelines and is summarized in Supplemental Table 1 [14, 15]. The tumors were stratified according to IHC receptor status into HR-positive (ER- and/or PR-positive and HER2-negative), HER2-positive, and triple-negative subgroups. The final histopathological results of surgical specimens were reviewed to determine pathological T and N categories. A pCR was defined as the absence of residual invasive tumor cells in the breast and axilla.

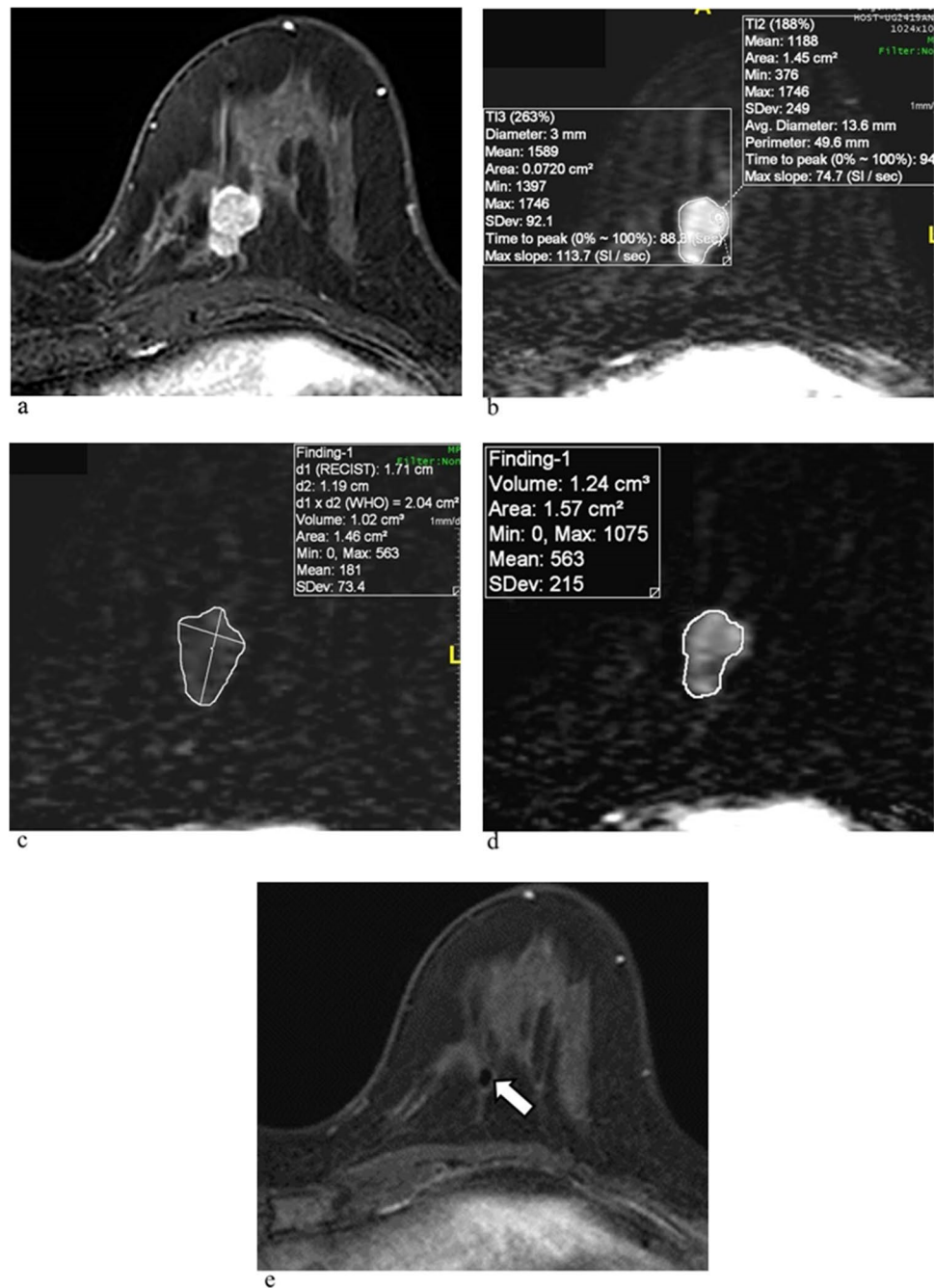
Statistical analysis

The clinicopathologic factors, ultrafast and conventional DCE-MRI features obtained from pretreatment MRI data, were compared on the basis of pCR. Continuous variables were compared using the Mann–Whitney *U* test or Student *t* test. Categorical variables were compared by using the χ^2 test or the Fisher exact test. Two-sided $p < 0.05$ was considered to indicate a statistically significant difference. For IHC subtypes, post hoc pairwise analysis was performed with a Bonferroni method for multiple comparison adjustment; $p < 0.017$ (0.05/3) was needed to for a statistically significant difference.

Logistic regression analysis was performed to investigate association between variables and pCR. Multivariable logistic regression was performed for variables with a p value < 0.05 at univariable analysis. We also performed separate logistic regression analysis for each IHC subgroups (HR-positive, HER2-positive, triple-negative). For the kinetic parameters that showed a significant difference, receiver operating characteristic (ROC) curve analysis was performed to determine the optimal cutoff values by using the maximum Youden index.

Intraclass correlation coefficient (ICC) was used to evaluate interobserver agreement and absolute tumor volume agreements between time points with the following interpretation: a value of 1.0 was considered perfect agreement; 0.81–0.99, almost perfect agreement; 0.61–0.80, substantial agreement; 0.41–0.60, moderate agreement; 0.21–0.40, fair agreement; and 0.20 or less, slight agreement [16]. All statistical analyses were performed with commercially available software (SPSS [version 25.0, IBM], SAS [version 9.4, SAS Inc.], and MedCalc [version 20.011, MedCalc Software]).

Fig. 2 Images in a 52-year-old woman with triple-negative invasive ductal carcinoma who achieved pCR after NAC. **a** Pretreatment axial conventional early contrast-enhanced MRI scan shows the enhancing breast cancer in the left upper inner breast. **b** Maximal slope was calculated by placing a circular ROI of 3 × 3 mm at the most rapidly enhancing part of the tumor, and also by manually placing a ROI over the enhancing portion of the tumor on ultrafast DCE-MRI. Tumor volume was measured on ultrafast DCE-MRI at time point U1 (**c**) and U2 (**d**), resulting in a U1/U2 volume ratio of 0.82. **e** Post-treatment axial conventional early contrast-enhanced MRI scan shows no residual enhancement around the clip marker, which had been previously inserted within the tumor (arrow)



Results

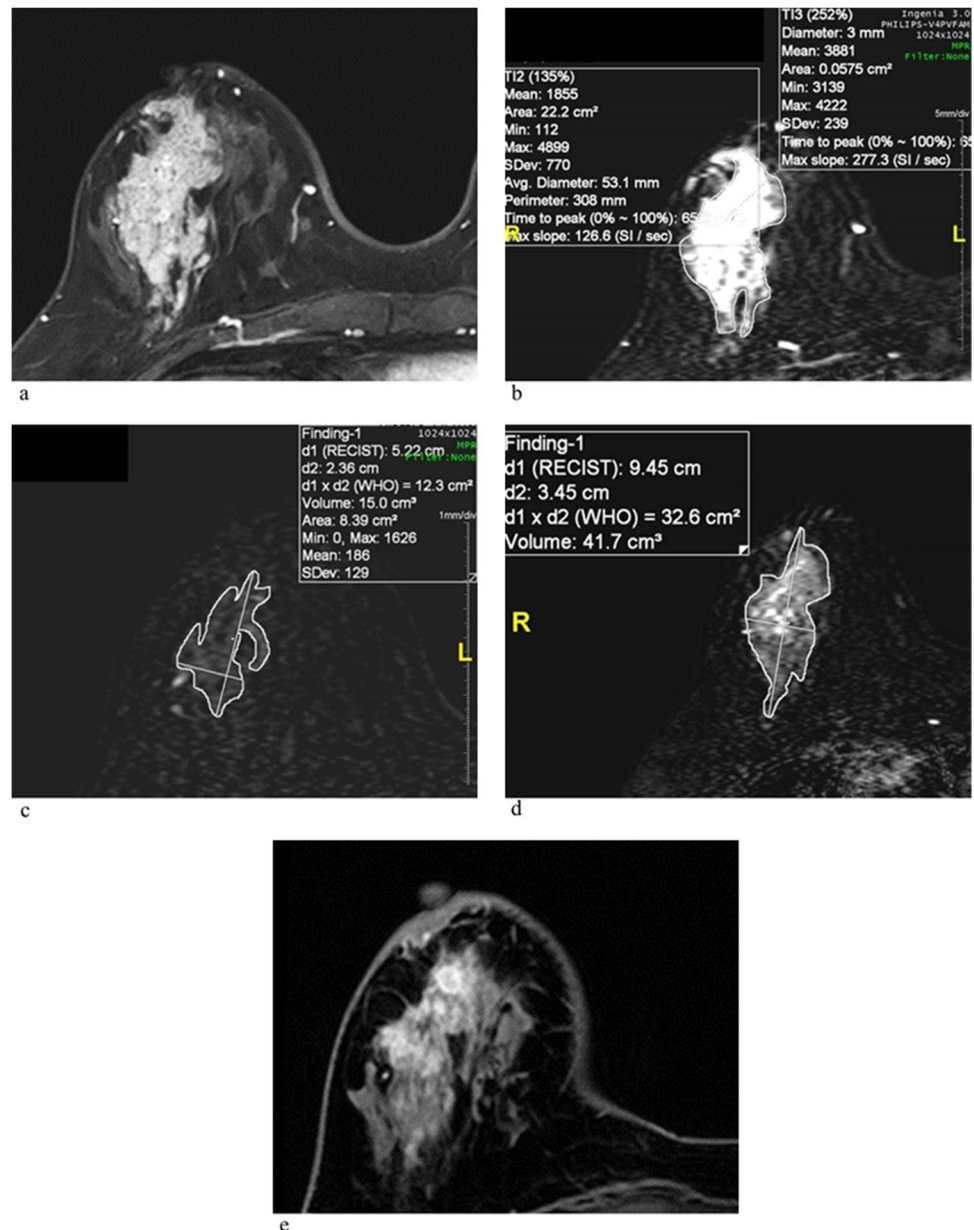
Baseline characteristics and pCR outcomes

Clinical and imaging characteristics of the 256 patients are shown according to pCR status in Table 2. Of the 256 cancers, 230 (89.8%) were invasive ductal carcinoma, 10 (3.9%) were invasive lobular carcinoma, 10 (3.9%) were mucinous carcinoma, 3 (1.2%) were invasive papillary carcinoma, and 3 (1.2%) were metaplastic carcinoma. According to IHC profiles, 84 (32.8%, 84 of 256) were classified as HR-positive,

85 (33.2%, 85 of 256) were HER2-positive, and 87 (34.0%, 87 of 256) were triple-negative breast cancer. Most HR-positive patients received taxane-containing NAC regimens, and HER2-positive patients received HER2 targeted therapy. In triple-negative cancers, most patients received anthracycline and taxane-based NAC. Further details are presented in Supplemental Table 2.

Of the 256 invasive breast cancers, 106 (41.4%) achieved pCR. The rate of pCR was significantly different between HR-positive and HER2-positive tumors (13.1% [11 of 84] vs. 63.5% [54 of 85], $p < 0.001$), and HR-positive and

Fig. 3 Images in a 54-year-old woman with HER2-positive invasive ductal carcinoma. **a** Pretreatment axial conventional early contrast-enhanced MRI scan shows heterogeneous non-mass enhancement in the right outer central breast. **b** Maximal slope was calculated by placing a circular ROI of 3×3 mm at the most rapidly enhancing part of the tumor, and also by manually placing a ROI over the enhancing portion of the tumor on ultrafast DCE-MRI. Tumor volume was measured on ultrafast DCE-MRI at time point U1 (**c**) and U2 (**d**), resulting in a U1/U2 volume ratio of 0.36. **e** Post-treatment axial conventional early contrast-enhanced MRI scan shows remaining nonmass enhancement. Surgery revealed residual invasive ductal carcinoma and in situ



triple-negative tumors (13.1% [11 of 84] vs. 47.1% [41 of 87], $p < 0.001$), but there was no significant difference between HER2-positive and triple-negative tumors (63.5% [54 of 85] vs. 47.1% [41 of 87], $p = 0.031$).

Analysis of all invasive breast cancer patients

Patients who failed to achieve pCR had a significantly higher proportion of clinically positive lymph nodes than those who achieved pCR (76.0% vs. 62.3%, $p = 0.018$) (Table 2). At univariable logistic regression analysis, clinical lymph node status was the only variable associated with pCR (OR, 0.521; 95% CI, 0.303, 0.897, $p = 0.019$). None of the

imaging parameters was associated with pCR when including all patients regardless of IHC subtype (Supplemental Table 3).

Analysis according to IHC subgroup

Among HR-positive tumors, 11 (13.1%, 11 of 84) achieved pCR. At univariable logistic regression analysis, a lower MS derived from ultrafast DCE-MRI (OR, 0.982; 95% CI, 0.966, 0.999, $p = 0.040$), lower peak enhancement (OR, 0.993; 95% CI, 0.987, 0.999, $p = 0.031$), and a lower percentage of wash-out based on conventional DCE-MRI kinetic analysis (OR, 0.904; 95% CI, 0.821, 0.995, $p = 0.039$) were associated with

Table 2 Clinical characteristics and MRI features based on pathological complete response status

Variable	Non-pCR group (<i>n</i> = 150)	pCR group (<i>n</i> = 106)	<i>p</i>
Patient age (years)*	50.8 ± 11.6	49.4 ± 10.5	0.344
Multiplicity			0.571
Single	91 (60.7)	68 (64.2)	
Multiple	59 (39.3)	38 (35.8)	
Clinical tumor size (mm)	32 (24–50.8)	30 (24–39)	0.324
Clinical lymph node			0.018
Negative	36 (24.0)	40 (37.7)	
Positive	114 (76.0)	66 (62.3)	
IHC subtype			<0.001
HR-positive	73 (48.7)	11 (10.4)	
HER2-positive	31 (20.7)	54 (50.9)	
Triple-negative	46 (30.7)	41 (38.7)	
MRI features			
Lesion type			0.749
Mass	89 (59.3)	65 (61.3)	
NME	61 (40.7)	41 (38.7)	
TTE (seconds)	6.5 (6.5–13)	6.5 (6.5–13)	0.766
MS (%/s)	110.4 (81.1–148.9)	116.3 (77.2–150.9)	0.762
MS_3mm (%/s)	170.7 (125.8–225.9)	183.4 (127.7–223.2)	0.727
Volume ratio U1/U2 (%)	0.6 (0.4–0.9)	0.7 (0.6–0.9)	0.104
Volume ratio U1/CAD (%)	0.4 (0.2–0.7)	0.5 (0.3–0.6)	0.364
Volume ratio U2/CAD (%)	0.8 (0.6–0.9)	0.7 (0.6–0.9)	0.174
Tumor volume U1 (cm ³)	3.1 (1.4–8.7)	2.7 (1.3–6.7)	0.423
Tumor volume U2 (cm ³)	5.6 (2.8–13.8)	4.6 (2.3–8.7)	0.101
CAD volume	8.8 (3.9–22.2)	6.9 (3.6–13.4)	0.080
Peak enhancement (%)	382.5 (292–515.5)	369 (278–506.8)	0.315
Percentage of washout (%)	13 (3–32)	13 (1.3–30.5)	0.699

Categorical data are numbers of tumors, with percentages in parentheses. Unless otherwise indicated, continuous data are median, with interquartile ranges in parentheses. *Data are means ± standard deviation. *pCR*, pathological complete response; *NME*, nonmass enhancement; *TTE*, time-to-enhancement; *MS*, maximal slope; *CAD*, computer-aided diagnosis; *U1*, the time point at which the lesion starts to enhance; *U2*, the subsequent time point after the lesion starts to enhance; *CAD volume*, total enhancing tumor volume calculated by the CAD system; *volume ratio U1/U2*, the ratio of tumor volume at U1 to volume at U2; *U1/CAD*, the ratio of tumor volume at U1 to volume calculated by the CAD system; *U2/CAD*, the ratio of tumor volume at U2 to volume calculated by the CAD system; *IHC*, immunohistochemistry; *HR*, hormone receptor; *HER2*, human epidermal growth factor receptor 2

pCR. MS_3mm showed borderline significance (OR, 0.989; 95% CI, 0.978, 1.000, *p* = 0.052) (Table 3). Due to the small number of pCR cases (*n* = 11) in this subgroup, multivariable analysis was not performed. On the basis of the results of ROC curve analysis, the optimal cutoff values for predicting pCR were as follows: MS, 118.6%/s (area under the curve [AUC]: 0.697 [95% CI: 0.587, 0.792], sensitivity: 90.9% [95% CI: 58.7, 99.8], specificity: 46.6% [95% CI: 34.8, 58.6], *p* = 0.007); peak enhancement, 261% (AUC: 0.733 [95% CI: 0.626, 0.824], sensitivity: 63.6% [95% CI: 30.8, 89.1], specificity: 83.6% [95% CI: 73.0, 91.2], *p* = 0.019); and percentage of washout, 1% (AUC: 0.772 [95% CI: 0.668, 0.857], sensitivity: 63.6% [95% CI: 30.8, 89.1], specificity: 80.8% [95% CI: 69.9, 89.1], *p* < 0.001).

Among HER2-positive tumors, 54 (63.5%, 54 of 85) achieved pCR. At univariable logistic regression analysis, only clinical lymph node status was associated with pCR (OR, 0.349; 95% CI, 0.123, 0.991, *p* = 0.048) (Table 3). None of the imaging parameters showed association with pCR in this subgroup.

Among triple-negative tumors, 41 (47.1%, 41 of 87) achieved pCR. At univariable logistic regression analysis, a higher volume ratio U1/U2 (OR, 11.787; 95% CI, 2.056, 67.539, *p* = 0.006) and a smaller clinical tumor size (OR, 0.962; 95% CI, 0.931, 0.994, *p* = 0.020) were associated with pCR. At multivariable analysis, the volume ratio U1/U2 (OR, 14.811; 95% CI, 2.228, 98.483, *p* = 0.005) and clinical tumor size (OR, 0.955; 95% CI,

Table 3 Univariable logistic regression analysis of variables associated with pCR in patients with HR-positive ($n = 84$) and HER2-positive invasive breast cancers ($n = 85$)

Subtype	HR-positive			HER2-positive			p
	Non-pCR group ($n = 73$)	pCR group ($n = 11$)	Odds ratio (95% CI)	Non-pCR group ($n = 31$)	pCR group ($n = 54$)	Odds ratio (95% CI)	
Patient age (years)*	49.1 ± 10.6	48.2 ± 14.1	0.993 (0.936–1.053)	51.8 ± 9.7	49.7 ± 9.3	0.976 (0.930–1.024)	0.976
Multiplicity			0.988				0.114
Single	40 (54.8)	6 (54.5)	Ref	14 (45.2)	34 (63.0)	Ref	
Multiple	33 (45.2)	5 (45.5)	1.010 (0.283–3.608)	17 (54.8)	20 (37.0)	0.484 (0.197–1.189)	
Clinical tumor size (mm)	30 (23–51)	30 (25.5–42.5)	0.995 (0.965–1.027)	36 (28–51.5)	34 (25.5–46)	0.988 (0.967–1.009)	0.265
Clinical lymph node			0.399				0.048
Negative	7 (9.6)	2 (18.2)	Ref	6 (19.4)	22 (40.7)	Ref	
Positive	66 (90.4)	9 (81.8)	0.477 (0.086–2.662)	25 (80.6)	32 (59.3)	0.349 (0.123–0.991)	
MR features							
Lesion type			0.239				0.115
Mass	39 (53.4)	8 (72.7)	Ref	21 (67.7)	27 (50.0)	Ref	
NME	34 (46.6)	3 (27.3)	0.430 (0.106–1.752)	10 (32.3)	27 (50.0)	2.100 (0.834–5.283)	
TTE (seconds)	6.5 (6.5–13)	13 (6.5–13)	1.131 (0.967–1.324)	6.5 (6.5–9.75)	6.5 (6.5–6.5)	0.939 (0.831–1.061)	0.311
MS (%/s)	115.8 (84.6–152.8)	87.6 (64.0–109.2)	0.982 (0.966–0.999)	126.4 (91.4–162.6)	120.5 (78.6–158.6)	0.998 (0.990–1.010)	0.642
MS_3mm (%/s)	176.1 (125.1–224)	139.4 (115.0–169.5)	0.989 (0.978–1.000)	187.1 (138.2–241)	187.9 (129.2–229.5)	1.000 (0.994–1.005)	0.865
Volume ratio U1/U2 (%)	0.6 (0.4–0.9)	0.7 (0.6–0.8)	4.330 (0.338–55.439)	0.7 (0.5–0.8)	0.6 (0.4–0.8)	0.213 (0.033–1.373)	0.104
Volume ratio U1/CAD (%)	0.4 (0.2–0.6)	0.5 (0.4–0.7)	2.933 (0.275–31.308)	0.5 (0.3–0.8)	0.4 (0.3–0.6)	1.037 (0.546–1.967)	0.912
Volume ratio U2/CAD (%)	0.8 (0.6–0.9)	0.7 (0.7–0.9)	1.190 (0.088–16.058)	0.8 (0.6–0.9)	0.7 (0.6–0.9)	1.250 (0.550–2.838)	0.595
Tumor volume U1 (cm ³)	2.8 (1.0–6.2)	1.8 (1.3–2.2)	0.864 (0.687–1.085)	5.9 (2.1–13.7)	2.8 (1.3–6.4)	0.981 (0.955–1.007)	0.154
Tumor volume U2 (cm ³)	4.7 (2.6–10.7)	2.7 (1.8–4.6)	0.860 (0.710–1.041)	10.1 (3.2–20.2)	5.5 (2.5–9.2)	0.984 (0.963–1.006)	0.162
CAD volume	7.1 (3.6–16)	4.2 (2–6.1)	0.915 (0.818–1.023)	15.2 (4.9–31.2)	7.3 (3.8–14.2)	0.982 (0.962–1.003)	0.085
Peak enhancement (%)	352 (292–483)	260 (161.5–363)	0.993 (0.987–0.999)	416 (318–525)	379.5 (304.5–475.5)	0.999 (0.997–1.002)	0.629
Percentage washout (%)	14 (5–32)	1 (0–9)	0.904 (0.821–0.995)	18 (3–39.5)	15 (3.3–35.8)	0.995 (0.974–1.016)	0.647

Categorical data are numbers of tumors, with percentages in parentheses. Unless otherwise indicated, continuous data are median, with interquartile ranges in parentheses. *Data are means ± standard deviation. CI, confidence interval; Ref, reference standard

Table 4 Univariable and multivariable logistic regression analysis of variables associated with pCR in patients with triple-negative invasive breast cancer ($n=87$)

Variable	Non-pCR group ($n=46$)	pCR group ($n=41$)	Univariable Odds ratio (95% CI)	Univariable p	Multivariable Odds ratio (95% CI)	Multivariable p
Patient age (years)*	52.8 ± 14.0	49.5 ± 11.1	0.979 (0.947–1.013)	0.226		
Multiplicity				0.197		
Single	37 (80.4)	28 (68.3)	Ref			
Multiple	9 (19.6)	13 (31.7)	1.909 (0.715–5.093)			
Clinical tumor size (mm)	32 (24–45.5)	26 (23–35)	0.962 (0.931–0.994)	0.020	0.955 (0.918–0.019 0.992)	
Clinical lymph node				0.305		
Negative	23 (50.0)	16 (39.0)	Ref			
Positive	23 (50.0)	25 (61.0)	1.562 (0.668–3.667)			
MR features						
Lesion type				0.314		
Mass	29 (63.0)	30 (73.2)	Ref			
NME	17 (37.0)	11 (26.8)	0.625 (0.251–1.560)			
TTE (seconds)	6.5 (6.5–6.5)	6.5 (6.5–13)	1.062 (0.950–1.187)	0.290		
MS (%/s)	94.2 (75.7–120.1)	125.5 (78.6–150.2)	1.006 (0.997–1.015)	0.197		
MS_3mm (%/s)	148.9 (125.2– 213.7)	191.5 (134.6–224)	1.002 (0.996–1.007)	0.529		
Volume ratio U1/U2 (%)	0.6 (0.4–0.9)	0.8 (0.7–1.0)	11.787 (2.056– 67.539)	0.006	14.811 (2.228–0.005 98.483)	
Volume ratio U1/CAD (%)	0.4 (0.2–0.7)	0.5 (0.4–0.7)	3.105 (0.772–12.493)	0.111		
Volume ratio U2/CAD (%)	0.8 (0.6–0.9)	0.7 (0.5–0.9)	0.939 (0.213–4.131)	0.934		
Tumor volume U1 (cm ³)	3.3 (1.5–11.6)	3.4 (2.0–8.1)	0.977 (0.936–1.020)	0.284		
Tumor volume U2 (cm ³)	6.0 (3.0–15.6)	4.0 (2.5–9.2)	0.969 (0.934–1.006)	0.097		
CAD volume	9.0 (4.6–22.3)	7.0 (4.1–12.8)	0.981 (0.958–1.005)	0.113		
Peak enhancement (%)	387.5 (284.8–556)	357 (282–535)	0.999 (0.997–1.001)	0.323		
Percentage washout (%)	6 (2–25.8)	15 (4–27)	1.003 (0.983–1.023)	0.763		

Categorical data are numbers of tumors, with percentages in parentheses. Unless otherwise indicated, continuous data are median, with interquartile ranges in parentheses. *Data are means ± standard deviation. *CI*, confidence interval; *Ref*, reference standard

0.918, 0.992, $p=0.019$) were independently associated with pCR (Table 4). On the basis of ROC curve analysis, the optimal cutoff value for volume ratio U1/U2 was 0.53 (AUC: 0.659 [95% CI: 0.550, 0.757], sensitivity: 92.7% [95% CI: 80.1, 98.5], specificity: 47.8% [95% CI: 32.9, 63.1], $p=0.008$).

Interobserver agreement for tumor volume

Tumor volume measured by ultrafast DCE-MRI showed almost perfect agreement between the two readers for both time point U1 and U2 (ICC=0.994 for tumor volume at U1; ICC=0.993 for tumor volume at U2). The ICC was 0.939 for tumor volume ratio U1/U2, indicating almost perfect agreement. In addition, tumor volumes measured at time point U2 showed better agreement with CAD-generated angiovolumes calculated from conventional DCE-MRI (ICC=0.929) than those measured at time point UI (ICC=0.760) (Supplemental Table 4).

Discussion

Although none of the pretreatment kinetic features was associated with pCR when analyzing the entire study population collectively, we found that different ultrafast DCE-MRI features were associated with pCR according to IHC subtype. Our study results suggest that although ultrafast DCE-MRI can aid in pCR prediction, a tailored approach of applying different parameters according to IHC subtype would be beneficial.

We found that a lower MS derived from ultrafast DCE-MRI, lower peak enhancement, and a lower percentage of washout based on conventional DCE-MRI were associated with pCR in HR-positive tumors. As previous studies have reported that a higher peak enhancement or MS were associated with poor histological prognostic factors and that the proportion of washout type was greater in patients achieving pCR, these results may seem unexpected [17]. However, such

differences can most likely be attributed to differences in study samples. To our knowledge, there are no studies that have specifically investigated associations between pretreatment MRI kinetic parameters and pCR in only HR-positive cancers. Most previous studies have encompassed invasive breast cancers of all IHC subtypes, of which HER2-positive or triple-negative tumors show both higher rates of aggressive kinetic features and pCR. In addition, although some previous studies have classified HR-positive/HER2-positive tumors as luminal B, these would not have been included in our HR-positive subgroup [10]. In contrast to HER2-positive and triple-negative invasive breast cancer, NAC is mainly performed for locally advanced cases in HR-positive/HER2-negative breast cancer. Therefore, our HR-positive subgroup would be primarily composed of relatively large and aggressive (i.e., node-positive) luminal A breast cancer, of which baseline tumor characteristics may differ from HR-positive tumors in general. In addition, due to the poor response to NAC in HR-positive tumors, the number of pCR cases was small ($n=11$). Future studies with larger study samples may be able to identify additional MRI predictors of response in this subgroup.

In the HER2-positive subgroup, only clinically negative lymph node status was associated with pCR. Our results are consistent with previous studies reporting association between clinical lymph node status and pCR in invasive breast cancer [18, 19]. Similar to previous studies [9, 10], the pCR rate was highest in this subgroup (63.5%). Considering the high pCR rate and that HER2-positive breast cancers have been reported to show significantly shorter bolus arrival time than luminal type cancer [20], differences in early pretreatment kinetic features may not be able to sufficiently differentiate pCR vs. non-pCR groups in these tumors.

In the triple-negative subgroup, we found that a smaller clinical tumor size was associated with pCR. Our results are consistent with previous studies, including a study reporting that the chance of pCR is 39.7% for clinical T2 triple-negative breast cancer and 26% for clinical T3 triple-negative breast cancer [21–23]. In addition, we found that a higher volume ratio U1/U2 at ultrafast DCE-MRI was associated with pCR in triple-negative breast cancers. In a previous study comparing size assessment between ultrafast and conventional DCE-MRI, tumor size at U2 was comparable to the histopathological tumor size, whereas the median tumor size at U1 was significantly smaller than tumor size at U2 [24]. Therefore, a high volume ratio U1/U2 indicates that the majority of the tumor shows very early enhancement. Multiple studies have reported association between rapid early enhancement kinetic parameters and tumor aggressiveness, such as high histological grade, hormonal receptor negativity, and high Ki-67 level [20, 25, 26]. Thus, tumors with a high volume ratio U1/U2 are likely mostly composed of aggressive components with high neovascularization that respond better to chemotherapy. Also, as triple-negative breast cancer has been

reported to have a low proportion of coexisting DCIS [27], early enhancement characteristics may more solely reflect characteristics of invasive components which are related with pCR. Similar to our results, a recent study also reported that diameters in the late phase of ultrafast DCE-MRI showed no significant difference with the extent of pathological residual IDC [28]. Therefore, our study results support the potential for ultrafast DCE-MRI to substitute delayed MRI phases while preserving accuracy in pCR prediction, possibly in a combined abbreviated protocol.

However, despite efforts to accurately predict pCR earlier, mid-treatment and post-treatment MRIs are still the current standard of care for evaluating treatment response to NAC [4, 29]. In a recent study, conventional kinetic features were shown to improve the performance of mid-treatment MRI in tumor response and prognosis prediction [29]. Likewise, ultrafast kinetic features may hold higher potential in aiding pCR prediction in mid-treatment MRI, as enhancement features further differ according to the degree of response. Further studies including comparison between ultrafast and conventional MRI kinetic features or combined models would be informative in better understanding the additive value of ultrafast sequences.

Our study has several limitations. First, a patient selection bias might have occurred due to the retrospective design of our single-institution study. Second, we used angio volumes calculated by a CAD system for tumor volume measurements at conventional DCE-MRI, which may be less accurate than manual segmentation [30]. Third, we did not evaluate tumor volumes beyond the time point of U2 at ultrafast MRI. However, a previous study reported that the median tumor sizes at U2 and at later time points were not significantly different from each other [24].

In conclusion, we found that an ultrafast DCE-MRI feature was associated with pCR in invasive breast cancer but specific features differed according to IHC subtype. A higher volume ratio of U1/U2 derived from ultrafast DCE-MRI was independently associated with pCR in triple-negative invasive breast cancer.

Supplementary Information The online version contains supplementary material available at <https://doi.org/10.1007/s00330-021-08530-4>.

Funding This study has received funding by a faculty research grant of Yonsei University College of Medicine for 2019 (6–2019-0178) and a Basic Science Research Program through the National Research Foundation of Korea (NRF) funded by the Ministry of Education (NRF-2017R1D1A1B03035995).

Declarations

Guarantor The scientific guarantor of this publication is Vivian Young-jean Park, MD, PhD, Assistant professor of the Department of Radiology, Severance Hospital, Yonsei University, College of Medicine.

Conflict of Interest The authors declare no competing interests.

Statistics and Biometry One of the authors (Hye Jung Shin) has significant statistical expertise.

Informed Consent Written informed consent was waived by the Institutional Review Board.

Ethical Approval Institutional Review Board approval was obtained.

Methodology

- Retrospective
- Observational
- Performed at one institution

References

1. Korde LA, Somerfield MR, Carey LA et al (2021) Neoadjuvant chemotherapy, endocrine therapy, and targeted therapy for breast cancer: ASCO guideline. *J Clin Oncol* 39:1485–1505
2. Mann RM, Cho N, Moy L (2019) Breast MRI: state of the art. *Radiology* 292:520–536
3. Scheel JR, Kim E, Partridge SC et al (2018) MRI, clinical examination, and mammography for preoperative assessment of residual disease and pathologic complete response after neoadjuvant chemotherapy for breast cancer: ACRIN 6657 Trial. *AJR Am J Roentgenol* 210:1376–1385
4. Hylton NM, Blume JD, Bernreuter WK et al (2012) Locally advanced breast cancer: MR imaging for prediction of response to neoadjuvant chemotherapy—results from ACRIN 6657/I-SPY TRIAL. *Radiology* 263:663–672
5. Gao Y, Heller SL (2020) Abbreviated and ultrafast breast MRI in clinical practice. *Radiographics* 40:1507–1527
6. Herrmann KH, Baltzer PA, Dietzel M et al (2011) Resolving arterial phase and temporal enhancement characteristics in DCE MRM at high spatial resolution with TWIST acquisition. *J Magn Reson Imaging* 34:973–982
7. Mann RM, Mus RD, van Zelst J, Geppert C, Karssemeijer N, Platel B (2014) A novel approach to contrast-enhanced breast magnetic resonance imaging for screening: high-resolution ultrafast dynamic imaging. *Invest Radiol* 49:579–585
8. Mus RD, Borelli C, Bult P et al (2017) Time to enhancement derived from ultrafast breast MRI as a novel parameter to discriminate benign from malignant breast lesions. *Eur J Radiol* 89:90–96
9. Cortazar P, Zhang L, Untch M et al (2014) Pathological complete response and long-term clinical benefit in breast cancer: the CTNeoBC pooled analysis. *Lancet* 384:164–172
10. Haque W, Verma V, Hatch S, Klimberg VS, Butler BE, Teh BS (2018) Response rates and pathologic complete response by breast cancer molecular subtype following neoadjuvant chemotherapy. *Breast Cancer Res Treat* 170:559–567
11. Morris EA, Comstock CE, Lee CH et al (2013) ACR BI-RADS® magnetic resonance imaging In: ACR BI-RADS® atlas, breast imaging reporting and data system. American College of Radiology, Reston, VA
12. Honda M, Kataoka M, Onishi N et al (2020) New parameters of ultrafast dynamic contrast-enhanced breast MRI using compressed sensing. *J Magn Reson Imaging* 51:164–174
13. van Roozendaal LM, de Wilt JH, van Dalen T et al (2015) The value of completion axillary treatment in sentinel node positive breast cancer patients undergoing a mastectomy: a Dutch randomized controlled multicentre trial (BOOG 2013–07). *BMC Cancer* 15:610
14. Hammond ME, Hayes DF, Dowsett M et al (2010) American Society of Clinical Oncology/College Of American Pathologists guideline recommendations for immunohistochemical testing of estrogen and progesterone receptors in breast cancer. *J Clin Oncol* 28:2784–2795
15. Wolff AC, Hammond ME, Hicks DG et al (2013) Recommendations for human epidermal growth factor receptor 2 testing in breast cancer: American Society of Clinical Oncology/College of American Pathologists clinical practice guideline update. *J Clin Oncol* 31:3997–4013
16. Landis JR, Koch GG (1977) The measurement of observer agreement for categorical data. *Biometrics* 33:159–174
17. Song SE, Cho KR, Seo BK, Woo OH, Jung SP, Sung DJ (2019) Kinetic features of invasive breast cancers on computer-aided diagnosis using 3T MRI data: correlation with clinical and pathologic prognostic factors. *Korean J Radiol* 20:411–421
18. Baron P, Beitsch P, Boselli D et al (2016) Impact of tumor size on probability of pathologic complete response after neoadjuvant chemotherapy. *Ann Surg Oncol* 23:1522–1529
19. Resende U, Cabello C, Ramalho SOB, Zeferino LC (2019) Prognostic assessment of breast carcinoma submitted to neoadjuvant chemotherapy with pathological non-complete response. *BMC Cancer* 19:601
20. Onishi N, Sadinski M, Hughes MC et al (2020) Ultrafast dynamic contrast-enhanced breast MRI may generate prognostic imaging markers of breast cancer. *Breast Cancer Res* 22:58
21. Gajdos C, Tartter PI, Estabrook A, Gistrak MA, Jaffer S, Bleiweiss IJ (2002) Relationship of clinical and pathologic response to neoadjuvant chemotherapy and outcome of locally advanced breast cancer. *J Surg Oncol* 80:4–11
22. Bonadonna G, Veronesi U, Brambilla C et al (1990) Primary chemotherapy to avoid mastectomy in tumors with diameters of three centimeters or more. *J Natl Cancer Inst* 82:1539–1545
23. Goorts B, van Nijnatten TJ, de Munck L et al (2017) Clinical tumor stage is the most important predictor of pathological complete response rate after neoadjuvant chemotherapy in breast cancer patients. *Breast Cancer Res Treat* 163:83–91
24. Kim SY, Cho N, Choi Y et al (2020) Ultrafast dynamic contrast-enhanced breast MRI: lesion conspicuity and size assessment according to background parenchymal enhancement. *Korean J Radiol* 21:561–571
25. Shin SU, Cho N, Kim SY, Lee SH, Chang JM, Moon WK (2020) Time-to-enhancement at ultrafast breast DCE-MRI: potential imaging biomarker of tumour aggressiveness. *Eur Radiol* 30:4058–4068
26. Goto M, Sakai K, Yokota H et al (2019) Diagnostic performance of initial enhancement analysis using ultra-fast dynamic contrast-enhanced MRI for breast lesions. *Eur Radiol* 29:1164–1174
27. Goh CW, Wu J, Ding S et al (2019) Invasive ductal carcinoma with coexisting ductal carcinoma in situ (IDC/DCIS) versus pure invasive ductal carcinoma (IDC): a comparison of clinicopathological characteristics, molecular subtypes, and clinical outcomes. *J Cancer Res Clin Oncol* 145:1877–1886
28. Kato E, Mori N, Mugikura S, Sato S, Ishida T, Takase K (2021) Value of ultrafast and standard dynamic contrast-enhanced magnetic resonance imaging in the evaluation of the presence and extension of residual disease after neoadjuvant chemotherapy in breast cancer. *Jpn J Radiol* 39:791–801
29. Yamaguchi A, Honda M, Ishiguro H et al (2021) Kinetic information from dynamic contrast-enhanced MRI enables prediction of residual cancer burden and prognosis in triple-negative breast cancer: a retrospective study. *Sci Rep* 11:10112
30. Song SE, Seo BK, Cho KR et al (2020) Preoperative tumor size measurement in breast cancer patients: which threshold is appropriate on computer-aided detection for breast MRI? *Cancer Imaging* 20:32

Publisher's Note Springer Nature remains neutral with regard to jurisdictional claims in published maps and institutional affiliations.